

RESEARCH PAPER

Enhancement the Structural and Electrical Properties of PVA by the Additive of Y_2O_3 and $SrCO_3$ Nanoparticles and Apply as the Antibacterial

Ali Salim Jwad *, Ali Razzaq Abdulridha

Department of Physics, College of Education for Pure Sciences, University of Babylon, Babylon, Iraq

ARTICLE INFO

Article History:

Received 24 January 2024

Accepted 21 March 2024

Published 01 April 2024

Keywords:

Electrical Characteristic

FESEM

NPs

PVA

$SrCO_3$

Y_2O_3

ABSTRACT

This work describes how to use the solution casting method to add varying amounts (0, 1, 2, 3, and 4) of Y_2O_3 and $SrCO_3$ nanoparticles (NPs) to polyvinyl alcohol (PVA) composites. The optical microscopy images showed the formation of networked channels inside the polymeric matrix as electrically charged particles, which became more intense at higher nanoparticle concentrations. With the use of field emission scanning electron microscopy (FESEM), the surface of the nanocomposite was examined. The Y_2O_3 and $SrCO_3$ nanoparticles were found to be consistently and equally distributed throughout the PVA polymer matrix. Fourier transformation spectroscopy (FTIR) was used to analyses the structural characteristics of the nanocomposite and gather data on molecular vibration. The polymer matrix interacted with the additional Y_2O_3 and $SrCO_3$ nanoparticles, according to FTIR analysis. Physical interactions between Y_2O_3 and $SrCO_3$ nanoparticles and the PVA polymer matrix have been demonstrated by the FTIR analysis. The dielectric constant and loss were found to be significant of (PVA/ Y_2O_3 / $SrCO_3$) nanocomposite decrease with increasing of frequency while, they are increase with content ratio of Y_2O_3 and $SrCO_3$ NPs. The A.C. conductivity of (PVA/ Y_2O_3 / $SrCO_3$) nanocomposite increase with increasing of frequency and concentration of Y_2O_3 and $SrCO_3$ NPs. Finally, the PVA/ Y_2O_3 / $SrCO_3$ nanocomposites were tested for the antibacterial against both gram positive Staphylococcus aureus (S. aureus) and gram-negative Escherichia coli (E. coli). The result obtained that the inhibition zone diameter increased with increasing Y_2O_3 and $SrCO_3$ NPs. The PVA/ Y_2O_3 / $SrCO_3$ nanocomposite exhibited antibacterial activity.

How to cite this article

Jwad A., Abdulridha A. Enhancement the Structural and Electrical Properties of PVA by the Additive of Y_2O_3 and $SrCO_3$ Nanoparticles and Apply as the Antibacterial. J Nanostruct, 2024; 14(2):481-491. DOI: 10.22052/JNS.2024.02.010

INTRODUCTION

Nanocomposites, created by combining different materials, structures, and compositions, display a broad spectrum of properties that are highly suitable for a variety of applications. As a result, there has been considerable focus on

multifunctional materials in the nanocomposite sector [1, 2].

Polyvinyl alcohol (PVA) is a polymer that has garnered considerable attention from researchers because of its distinctive physical and chemical properties [3]. PVA is a multifunctional polymer

* Corresponding Author Email: pure.ali.razaq@uobabylon.edu.iq



that is utilized in various industries. The main factors that contribute to this phenomenon are their extraordinary optical properties, lightweight nature, and great mechanical qualities. Polyvinyl alcohol (PVA) is extensively utilized in various applications such as adhesives, drug delivery systems, coatings, and fuel cells. Because of the strong hydrogen bonds produced by hydroxyl groups, both internally and externally, PVA exhibits a high melting point that roughly matches its breakdown temperature. Due to this particular attribute, the melting procedure of PVA presents difficulties, which is why it is more beneficial to handle it by utilizing water-based solutions [4]. Because of its compatibility with the human body, it can also be used as a therapeutic substance [5]. Furthermore, PVA possesses the capacity to selectively adsorb metallic ions, including copper, palladium, and mercury. Polyvinyl alcohol (PVA) is a polymer represented by the chemical formula (C₂H₄O)_x. The substance exhibits a density within the range of 1.19 to 1.31 g/cm³ and a melting point of 230°C. This thermoplastic polymer experiences rapid breakdown when exposed to temperatures exceeding 200°C. The substance's structure is flexible and is defined by the existence of C–O–C connections. Furthermore, it possesses the capability to undergo dissolution in organic solvents, a propensity to interact with water, a structure characterized by crystals, and the potential to provide self-lubrication [6].

Yttrium oxide (Y₂O₃) is a highly significant substance in the field of advanced ceramics. Furthermore, (Y₂O₃) is favoured as a host material because of its exceptional chemical durability, elevated thermal stability, strong refractory property, resistance to corrosion, low phonon energy, and high refractive index [7]. Y₂O₃ (III) oxide, also referred to as yttria, diyttrium trioxide, yttrium sesquioxide, is an oxide that is stable in air and insoluble in water. It has diverse applications in the fields of material science and inorganic chemistry [8].

Strontium carbonate (SrCO₃) has a high dielectric constant, dispersion frequency constant, and low temperature coefficient, making it a promising chemical [9]. Strontium carbonate is essential to the electrical and glass industries [10]. As a bio-crystallization model, strontium carbonate's unusual crystal structure has been extensively studied [11]. Self-assembly monolayers [12], thermos evaporated stearic membrane [13],

and polyanionic additives [14] have been used to improve the production of crystalline SrCO₃ from water [15].

This work focuses on the synthesis of a nanocomposite consisting of PVA/Y₂O₃/SrCO₃ and the subsequent investigation of its structural and electrical properties and apply as the antibacterial.

MATERIALS AND METHODS

1g of PVA was dissolved in 50 mL of distilled water firstly for 30 minutes at RT, then continue for another 20 minutes under 75-80°C using magnetic stirrer until to PVA solvent. The resulting solution was cast onto clean glasses Petri dish and kept it under air at RT for 240h for drying process till the solvent gets completely evaporated. PVA with different concentration for Y₂O₃ and SrCO₃ NPs (0, 1, 2, 3 and 4) wt.% were fellow the same procedure to prepare nanocomposite films. The thickness of the produced films was about 0.12 mm.

To show the chemical make-up of the samples that were prepared, FTIR (Bruker business, type vertex -70 spectrometer, German origin) was used at room temperature, covering the range of 4000-500 cm⁻¹. To determine the surface morphology of the films, researchers used a (FESEM, INSPECT S50, firm, Japan origin, type FEI Customer ownership) and optical microscope (OM) provided by Olympus (Top View, type Nikon-73346). The dielectric characteristic were studied at (f=100 Hz to 5 ×10⁶ Hz) by LCR meter (HIOKI 3532-50 LCR HI TESTER).

The dielectric constant, ϵ' is given by [16]

$$\epsilon' = C_p d / \epsilon_0 A \quad (1)$$

wherever, C_p is capacitance of matter, thickness (d in cm), A=(in cm²). Dielectric loss, ϵ'' is calculated by [17]:

$$\epsilon'' = C_p d / \epsilon_0 A \quad (2)$$

Wherever, D: dispersion factor. The A.C electrical conductivity is determined by [18]:

$$\sigma_{A.C} = 2\pi f \epsilon' D \epsilon_0 \quad (3)$$

RESULT AND DISCUSSION

The optical microscope reveals changes in the surface morphology of (PVA/ Y₂O₃/

$SrCO_3$) nanocomposites. Fig. 1 depicts the nanocomposites (PVA/ Y_2O_3 / $SrCO_3$) captured using an optical microscope (OM) at a 10x magnification. The image depicts the organization of Y_2O_3 and $SrCO_3$ nanoparticles in the (PVA/ Y_2O_3 / $SrCO_3$) nanocomposite. At lower concentrations, the Y_2O_3 and $SrCO_3$ nanoparticles aggregate to form clusters. Increasing the concentrations of Y_2O_3 and

$SrCO_3$ nanoparticles in the (PVA) polymer results in the formation of a network of pathways within the polymer. These pathways allow charge carriers to flow, hence causing a modification in the material characteristics. This behavior agrees with [19,20].

FESEM is used for the purpose of examining the distribution of nanoparticles within the polymer, and then verifying the effect of those

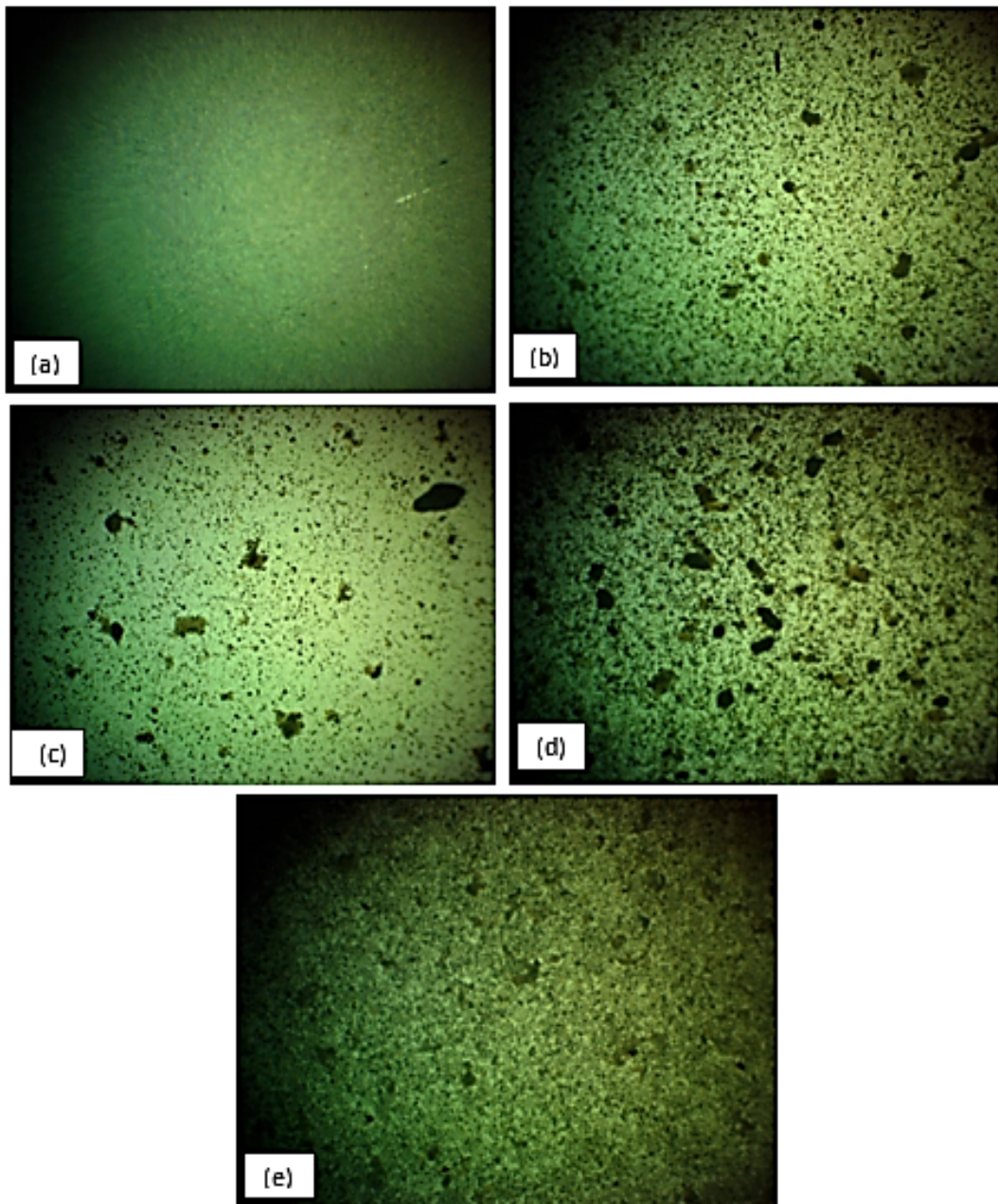


Fig. 1. Optical microscope for the (a) pure PVA, (b) 1 wt.% Y_2O_3 and $SrCO_3$ NPs, (c) 2 wt.% Y_2O_3 and $SrCO_3$ NPs, (d) 3 wt.% Y_2O_3 and $SrCO_3$ NPs, (e) 4wt.% Y_2O_3 and $SrCO_3$ NPs

particles of $Y_2O_3/SrCO_3$ on those nanocomposites. Fig. 2 shows FESEM images of films made from (PVA/ $Y_2O_3/SrCO_3$) nanocomposites with varying

amounts of Y_2O_3 and $SrCO_3$ NPs with a scale 1 μm . FESEM images of pure PVA polymer show that the surface is smooth and homogenous, which

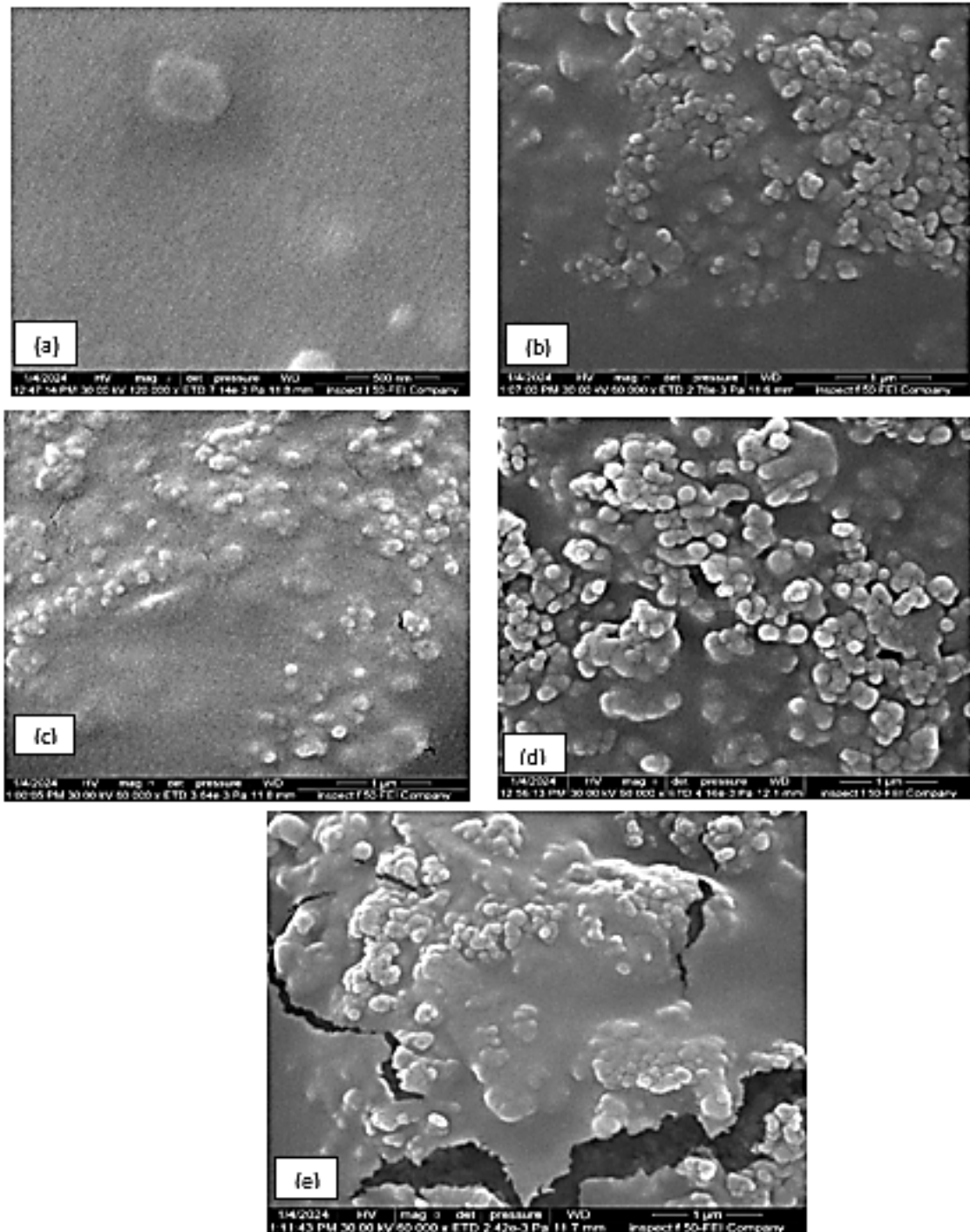


Fig. 2. FESEM images for the (a) pure PVA, (b) 1 wt.% Y_2O_3 and $SrCO_3$ NPs, (c) 2 wt.% Y_2O_3 and $SrCO_3$ NPs, (d) 3 wt.% Y_2O_3 and $SrCO_3$ NPs, (e) 4wt.% Y_2O_3 and $SrCO_3$ NPs

mean the successful this method to fabricated this film. Many Y_2O_3 and $SrCO_3$ particles, at lesser concentrations, are broadly disseminated

throughout the surface of the nanocomposite and are finely dispersed without aggregating. On the surface, nanoparticles are dispersed at random

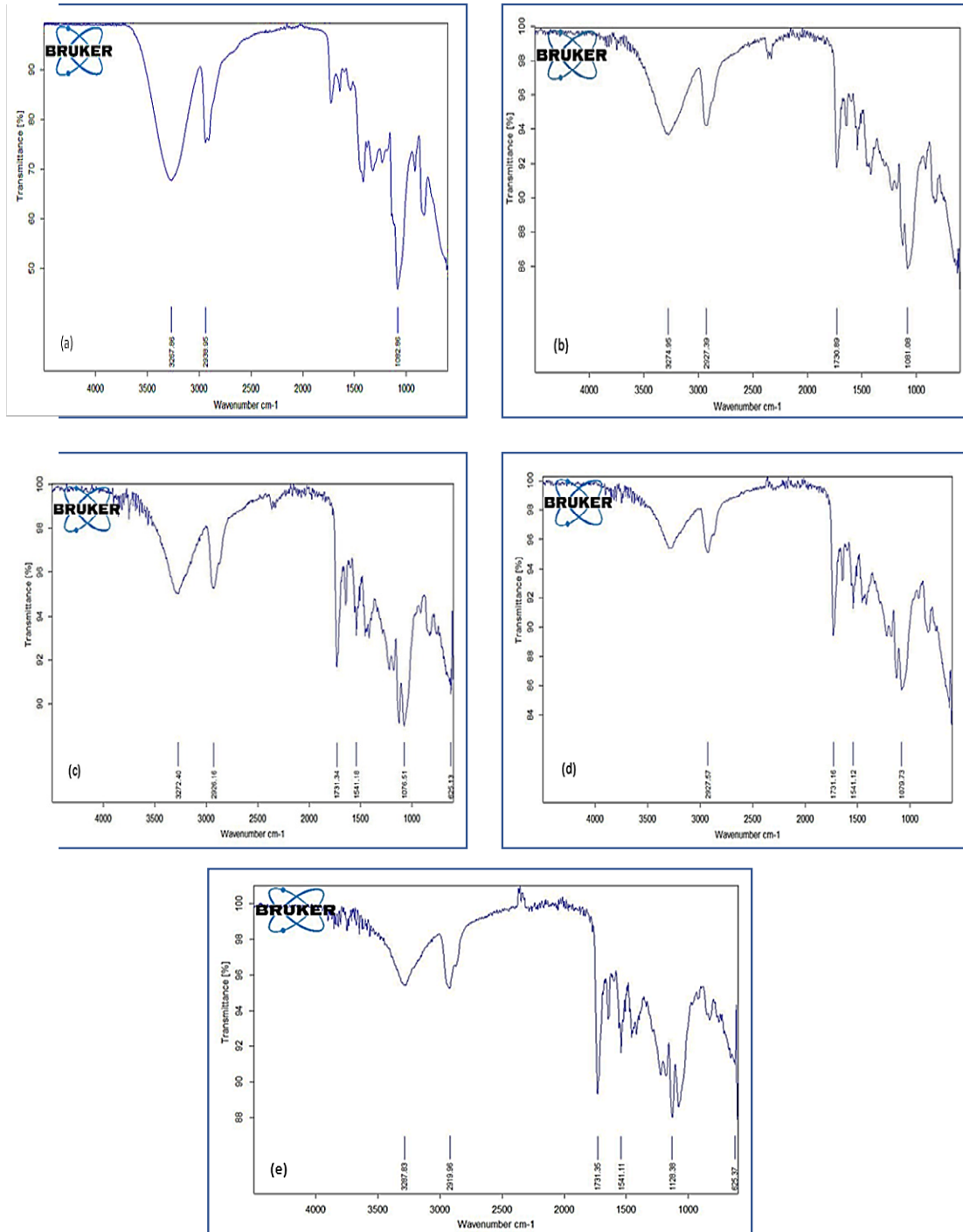


Fig. 3. FTIR spectrum for the (a) pure PVA, (b) 1 wt.% Y_2O_3 and $SrCO_3$ NPs, (c) 2 wt.% Y_2O_3 and $SrCO_3$ NPs, (d) 3 wt.% Y_2O_3 and $SrCO_3$ NPs, (e) 4wt.% Y_2O_3 and $SrCO_3$ NPs

and take on the shape of spheres, much like grains. When Y_2O_3 and $SrCO_3$ NPs are present in high concentrations, the nanoparticles aggregate and cluster, suggesting that there may be interaction between the two substances. This result is agreed with researches [21].

The freshly synthesized pure PVA and PVA/ Y_2O_3 / $SrCO_3$ nanocomposite were characterized using FTIR. Fig. 3 shows the FTIR spectra of pure PVA and PVA with Y_2O_3 and $SrCO_3$ nanoparticle concentrations from 500 to 4000 cm^{-1} . Pure PVA has a large absorption band at 3272.40 cm^{-1} due to the stretching vibration of the alcohol group

(OH) in the polymer matrix chain [22]. The C-H group has symmetric stretching vibrations at 2926.16 cm^{-1} . The stretching vibration of the C=C bond was observed at 1731.34 cm^{-1} , while the bending vibration of the O-H bond was observed at 1661.22 cm^{-1} . At 1541.18 cm^{-1} , chitosan absorbs due to its amino group stretching vibration. A bending vibration was observed at 1441.23 cm^{-1} for the C-H group. Infrared Spectroscopy was used to measure crystallinity by analyzing the peak at 1128.38 cm^{-1} [23, 24]. Crystalline polymeric chains impact this peak's magnitude. According to the literature [25, 26], this peak represents

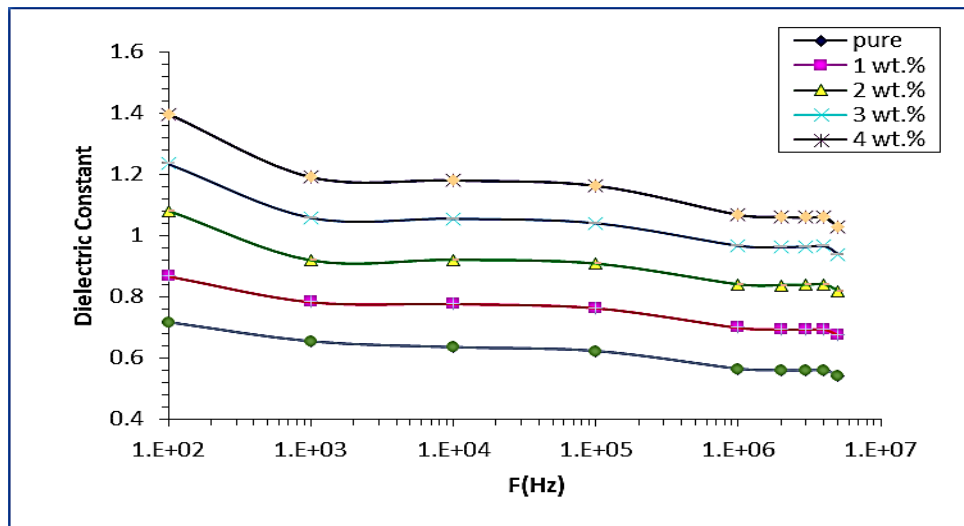


Fig. 4. Difference of the ϵ' of (PVA/ Y_2O_3 / $SrCO_3$) nanocomposites with frequency (Hz).

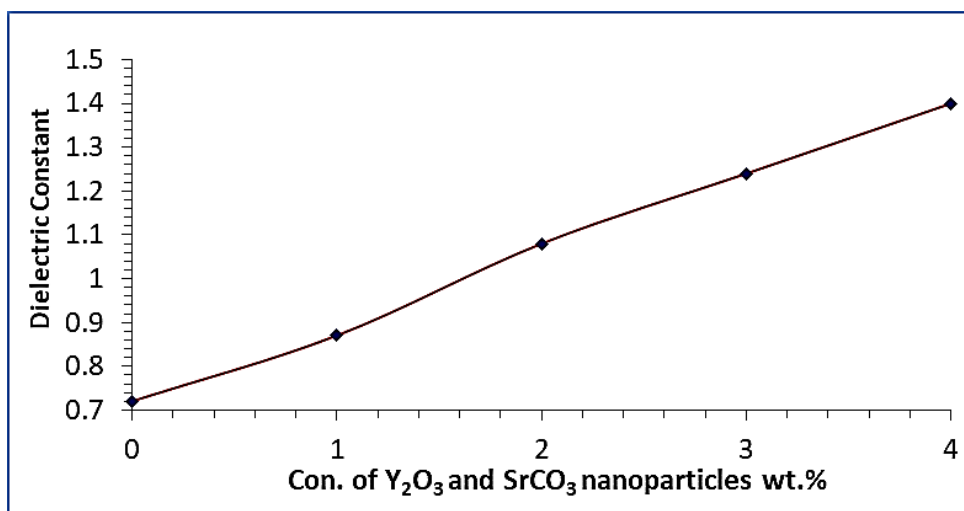


Fig. 5. Disparity of ϵ' with content of Y_2O_3 and $SrCO_3$ NPs at 100Hz

the symmetric C-C bond stretching mode or C-O bond stretching in a specific chain region. Two neighboring OH groups on the same side of the carbon chain plane form an intramolecular hydrogen bond [23]. The C-O stretching vibrations occurred at 1082.86 cm^{-1} . Peaks at 845.02 and

625.13 cm^{-1} correlate with powerful C-O-C and modest C=C bending vibrations [27].

The additive concentration (1, 2, 3, and 4) wt. % of Y_2O_3 and $SrCO_3$ NPs to PVA polymer in images b, c, d, and e changed some band intensities and shifted others. This graphic shows that Y_2O_3 and

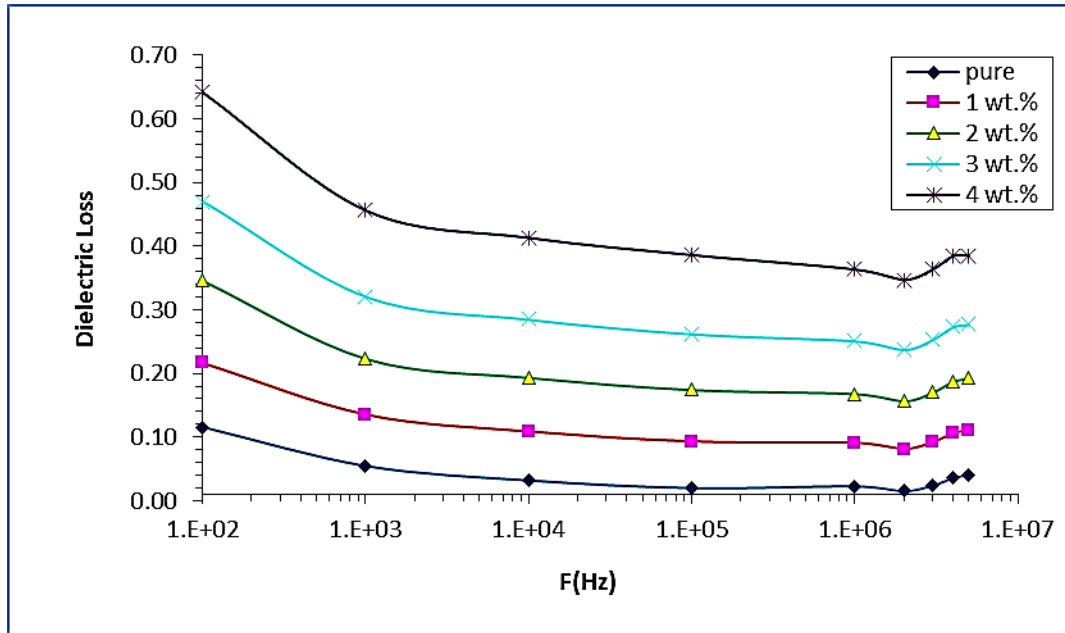


Fig. 6. Difference of the ϵ'' of (PVA/ Y_2O_3 / $SrCO_3$) nanocomposites with frequency (Hz).

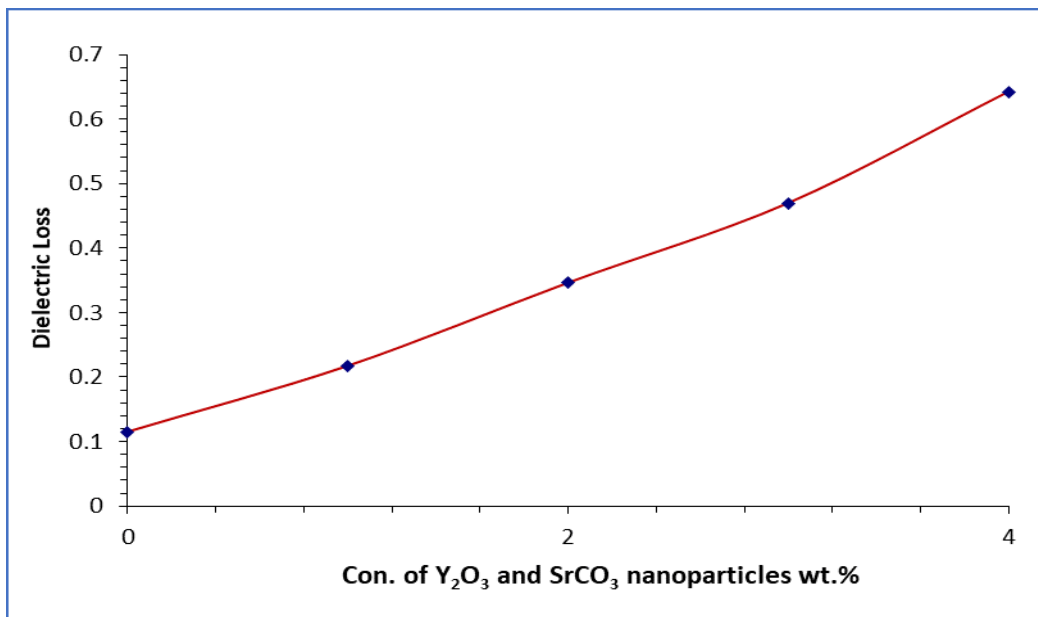


Fig. 7. Difference of ϵ'' with content σ_{AC} of Y_2O_3 and $SrCO_3$ NPs at 100Hz

$SrCO_3$ NPs interact with polymer matrix. The FTIR showed no interactions between PVA polymer matrix and Y_2O_3 and $SrCO_3$ NPs. This outcome matches researchers [28].

The dielectric constant was determined using equation 1. The frequency-dependent fluctuation of the dielectric constant for all specimens of the (PVA/ Y_2O_3 / $SrCO_3$) nanocomposite is illustrated

in Fig. 4. The results indicate a reduction in the dielectric constant with increasing applied frequency, attributed to the varying polarization states. However, at lower frequencies, the polarization of the space charge significantly contributes to increasing the dielectric constant. As the frequency of the electrical field increases, the influence of polarization on the frequency

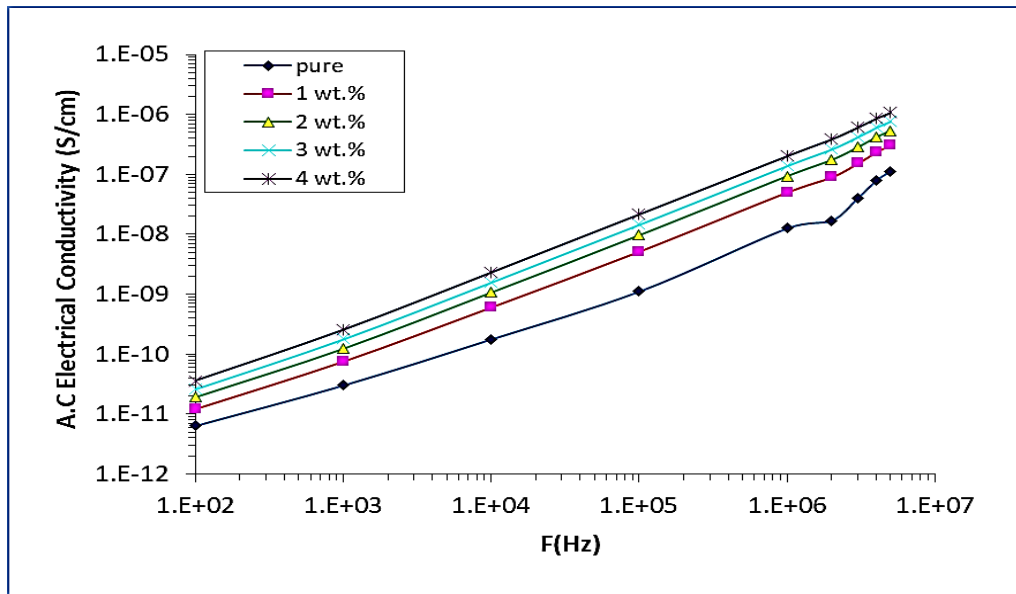


Fig. 8. Difference of the with frequency (Hz) for (PVA/ Y_2O_3 / $SrCO_3$) nanocomposites.

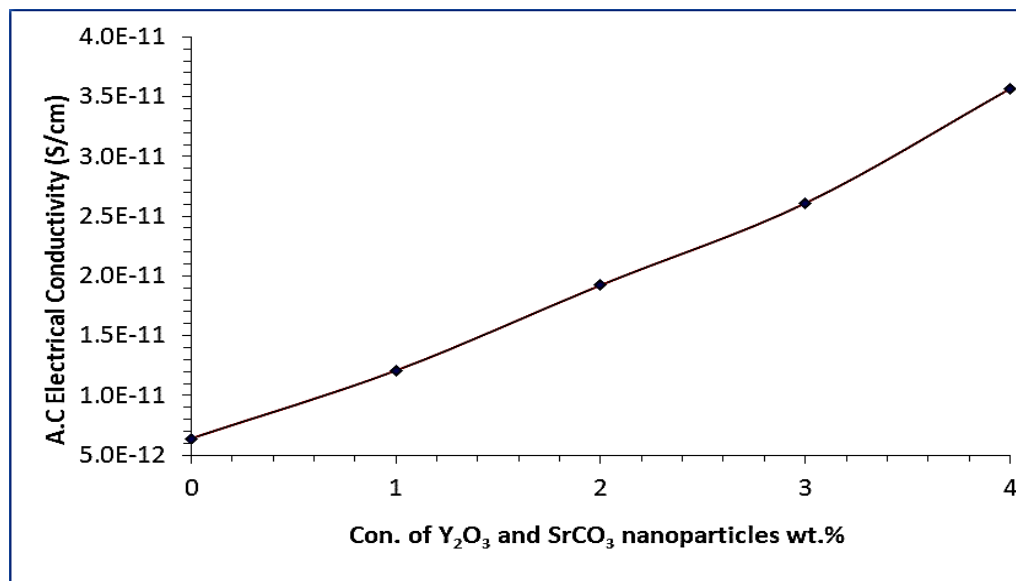


Fig. 9. Difference of with content of Y_2O_3 and $SrCO_3$ NPs at 100Hz

increase becomes less significant and more noticeable. As a result of this activity, the dielectric constant values decrease for all samples, which in turn causes various forms of polarizations to occur at higher frequencies. This phenomenon arises from the difference in mass between an ion and an electron. Electronic polarization is the only type of polarization that can occur at higher frequencies because of the difference in mass. This difference allows electrons to respond to fluctuations in the field, even at very high frequencies [29].

Fig. 5 demonstrates the impact of Y_2O_3 and $SrCO_3$ nanoparticles on the dielectric constant at a frequency of 100 Hz. The relationship between the dielectric constant and the concentration of Y_2O_3 and $SrCO_3$ NPs is clearly evident, as the dielectric constant increases proportionally with an increase in concentration. This could be attributed to the formation of a cohesive network by Y_2O_3 and $SrCO_3$ nanoparticles within the nanocomposite. The microscopic photographs of these nanocomposites clearly demonstrated this. This discovery exhibits

same behavior as that demonstrated in [30, 31].

The dielectric loss of nanocomposites was determined using equation 2. The Fig. 6 displays the frequency-dependent dielectric loss of the nanocomposite ($PVA/Y_2O_3/SrCO_3$). This graph illustrates that the dielectric loss of nanocomposites ($PVA/Y_2O_3/SrCO_3$) diminishes as the applied electric field increases. An elevated concentration of Y_2O_3 and $SrCO_3$ nanoparticles leads to a corresponding rise in the dielectric loss. As the frequency rises, there is a relatively small alteration in the level of dielectric loss. At high frequencies, many forms of polarization can occur [32]. The Fig. 7 illustrates that an growth in the content of Y_2O_3 and $SrCO_3$ results in an rise in the amount of ionic charge carriers. This, in turn, leads to an increase in the value of dielectric loss. This behavior becomes evident as the weight percentage of nanoparticles is raised. This is agreed with the results of researchers [33]

In order to find the A.C. electrical conductivity, its variation with regard to relation (3) was



Fig. 10. Image for inhibition zones of $PVA/Y_2O_3/SrCO_3$ nanocomposites with different concentration on *S. aureus* and *E. coli*

Table 1. Diameter of inhibition zone (mm) of $PVA/Y_2O_3/SrCO_3$ nanocomposites on *S. aureus* and *E. coli*

Concentration of $Y_2O_3/SrCO_3$ NPs	<i>E. Coli</i>	<i>S. Aureus</i>
0	0	0
1	0	0
2	16	15
3	18	17
4	20	19

computed. For the (PVA/ Y_2O_3 / $SrCO_3$) composite, the frequency-to- σ_{AC} relationship is shown in Fig. 8. The graph shows that when the frequency goes up, the electrical conductivity goes up as well. Reasons for this include localized charge carrier mobility and higher-level conduction band stimulation. Two factors that impact the electrical conductivity of alternating current (A.C.) are the movement of the main chain and the movement of ions. Specifically, the increase in σ_{AC} at low frequencies can be attributed to interfacial polarization, while the increase in conductivity at intermediate and high frequencies is caused by the flow of electrons. The data presented in Fig. 9 indicate that higher concentrations of Y_2O_3 and $SrCO_3$ NPs in nanocomposites lead to an elevated conductivity of the nanocomposites. This phenomenon arises due to an augmentation in the quantity of ionic charge carriers, along with the establishment of an uninterrupted network of Y_2O_3 and $SrCO_3$ nanoparticles within the composites. These results agree with other [33].

We assessed the antibacterial efficacy of PVA/ Y_2O_3 / $SrCO_3$ nanocomposites against both gram-negative *Escherichia coli* (*E. coli*) and gram-positive *Staphylococcus aureus* (*S. aureus*). The results of these tests at the various concentrations are shown in Fig. 10. The figure illustrates that the nanocomposite films exhibited a larger inhibition zone against gram-positive (*S. aureus*) compounds in comparison to gram-negative (*E. coli*) compounds. Table 1 illustrates how the inhibitory zone's diameter increases as graphene nanoparticle concentration rises, peaking at 18 mm for gram-negative bacteria (*E. coli*). The antibacterial properties of nanostructures are assumed to be caused by reactive oxygen species (ROS) generated by nanoparticles. Positive charges are present in nanocomposite nanoparticles, while negative charges are present in bacteria. Because of this, the bugs will be instantly killed by oxidation brought on by electromagnetic contact. Bacterial proteins and DNA most likely break down due to singlet oxygen ($^1O^2$). Reactive oxygen species (ROS) are primarily responsible for the antibacterial properties of nanocomposites containing nanoparticles. These radicals include superoxide ($O^{\cdot-}$), hydroxyl (OH), and hydrogen peroxide (H_2O_2) [34].

CONCLUSION

This study provides a concise overview of

a very efficient casting technique employed in the manufacturing of PVA/ Y_2O_3 / $SrCO_3$ nanocomposites. The OM images displayed the formation of interconnected channels inside the polymeric matrix due to the presence of electrically charged particles, which became more pronounced with higher concentrations of nanoparticles. The examination using Field Emission Scanning Electron Microscopy (FESEM) showed that the Y_2O_3 and $SrCO_3$ nanoparticles were evenly spread and uniformly distributed within the polymer PVA matrix. FTIR analysis conclusively verified the existence of a discernible interaction between Y_2O_3 / $SrCO_3$ and the PVA polymer matrix. The PVA/ Y_2O_3 / $SrCO_3$ nanocomposites' dielectric constant and dielectric loss reduction as the frequency of the applied electric field increases. In contrast, the electrical conductivity of alternating current increases with frequency. The dielectric constant, dielectric loss and the conductivity of PVA/ Y_2O_3 / $SrCO_3$ nanocomposites at all concentrations growth with increasing concentrations of Y_2O_3 and $SrCO_3$ nanoparticles. Finally, the PVA/ Y_2O_3 / $SrCO_3$ nanocomposites were examined as antibacterial against gram-positive (*Staphylococcus aureus*) and gram-negative (*Escherichia coli*) and exhibited that the inhibition zone diameter increments with the rise in Y_2O_3 and $SrCO_3$ content. The nanocomposite exhibited activity against antibacterial.

CONFLICT OF INTEREST

The authors declare that there is no conflict of interests regarding the publication of this manuscript.

REFERENCES

1. Moriche R, Sánchez M, Jiménez-Suárez A, Prolongo SG, Ureña A. Electrically conductive functionalized-GNP/epoxy based composites: From nanocomposite to multiscale glass fibre composite material. *Composites Part B: Engineering*. 2016;98:49-55.
2. Doagou-Rad S, Islam A, Merca TD. An application-oriented roadmap to select polymeric nanocomposites for advanced applications: A review. *Polym Compos*. 2019;41(4):1153-1189.
3. Mohammed MK, Abbas MH, Hashim A, Rabee BH, Habeeb MA, Hamid N. Enhancement of Optical Parameters for PVA/PEG/ Cr_2O_3 Nanocomposites for Photonics Fields. *Revue des composites et des matériaux avancés*. 2022;34(4):205-209.
4. Elhosiny Ali H, Abdel-Aziz M, Mahmoud Ibrahim A, Sayed MA, Abd-Rabboh HSM, Awwad NS, et al. Microstructure Study and Linear/Nonlinear Optical Performance of Bi-Embedded PVP/PVA Films for Optoelectronic and Optical Cut-Off Applications. *Polymers*. 2022;14(9):1741.
5. Hayder N, Hashim A, Habeeb MA, Rabee BH, Hadi AG,

- Mohammed MK. Analysis of Dielectric Properties of PVA/PEG/ In_2O_3 Nanostructures for Electronics Devices. *Revue des composites et des matériaux avancés*. 2022;32(5):261-264.
6. Refaat D, Mosa E, Fikry M, Omar M. A novel polyvinyl alcohol/polyethylene glycol (PVA/PEG) polymeric blend doped with graphene oxide for energy storage devices. *ERU Research Journal*. 2024;0(0):0-0.
 7. Habeeb MA, Hamza LA. Structural, Optical and D.C Electrical Properties of (PVA-PVP- Y_2O_3) Films and Their Application for Humidity Sensor. *Journal of Advanced Physics*. 2017;6(1):1-9.
 8. Mills SJ, Kartashov PM, Ma C, Rossman GR, Novgorodova MI, Kampf AR, Raudsepp M. Yttriaite-(Y): The natural occurrence of Y_2O_3 from the Bol'shaya Pol'ya River, Subpolar Urals, Russia. *Am Mineral*. 2011;96(7):1166-1170.
 9. Márquez-Herrera A, Ovando-Medina VM, Castillo-Reyes BE, Meléndez-Lira M, Zapata-Torres M, Saldaña N. A novel synthesis of $SrCO_3$ - $SrTiO_3$ nanocomposites with high photocatalytic activity. *J Nanopart Res*. 2014;16(12).
 10. Alavi MA, Morsali A. Syntheses and characterization of $Sr(OH)_2$ and $SrCO_3$ nanostructures by ultrasonic method. *Ultrason Sonochem*. 2010;17(1):132-138.
 11. Küther J, Nelles G, Seshadri R, Schaub M, Butt H-J, Tremel W. Templated Crystallisation of Calcium and Strontium Carbonates on Centred Rectangular Self-Assembled Monolayer Substrates. *Chemistry - A European Journal*. 1998;4(9):1834-1842.
 12. Küther J, Bartz M, Seshadri R, Vaughan GBM, Tremel W. Crystallization of $SrCO_3$ on a self-assembled monolayer substrate: an in-situ synchrotron X-ray study. *J Mater Chem*. 2001;11(2):503-506.
 13. Sastry M, Kumar A, Damle C, Sainkar SR, Bhagwat M, Ramaswamy V. Crystallization of $SrCO_3$ within thermally evaporated fatty acid films: unusual morphology of crystal aggregates. *CrystEngComm*. 2001;3(21):81.
 14. Cai Q, Ma H. Recent Advances of Chiral Hypervalent Iodine Reagents. *Acta Chim Sinica*. 2019;77(3):213.
 15. Yu J, Guo H, Cheng B. Shape evolution of $SrCO_3$ particles in the presence of poly-(styrene-alt-maleic acid). *J Solid State Chem*. 2006;179(3):800-803.
 16. Haiba AS, Gouda OE-s, Mahmoud SF, El-gendy AA. Improving the Dielectric Properties of High Density Polyethylene by Incorporating Clay-Nanofiller. *TELKOMNIKA (Telecommunication Computing Electronics and Control)*. 2014;12(4):763.
 17. Shivashankar H, Mathias KA, Sondar PR, Shrishail MH, Kulkarni SM. Study on low-frequency dielectric behavior of the carbon black/polymer nanocomposite. *Journal of Materials Science: Materials in Electronics*. 2021;32(24):28674-28686.
 18. Al-Rubaye SAJ, A. Al-Isawi N, Abdulridha AR. Preparation and Study the Electrical and Optical Properties for (PVA-PEG- Sr_2O_3) Nanocomposites. *Neuroquantology*. 2021;19(10):47-55.
 19. Abid AA, Al-nesrawy SH, Abdulridha AR. New Fabrication (PVA-PVP-C. B) Nanocomposites: Structural and Electrical Properties. *Journal of Physics: Conference Series*. 2021;1804(1):012037.
 20. Shanmugam G, Isaiyah MVG. Low cost and facile preparation of $Al(NO_3)_3$ doped PVA-PEG polymer electrolyte films for electrochemical applications. *International Journal of ChemTech Research*. 2019;12(04):150-157.
 21. Rajeswari N, Selvasekarapandian S, Karthikeyan S, Prabu M, Hirankumar G, Nithya H, Sanjeeviraja C. Conductivity and dielectric properties of polyvinyl alcohol-polyvinylpyrrolidone poly blend film using non-aqueous medium. *Journal of Non-Crystalline Solids*. 2011;357(22-23):3751-3756.
 22. Jassim HH, Hashim FS. Synthesis of (PVA/PEG: ZnO and Co_3O_4) Nanocomposites: Characterization and Gamma Ray Studies. *Neuroquantology*. 2021;19(4):47-56.
 23. Negim E, Rakhmetullayeva R, Yeligbayeva G, Urkimbaeva P, Primzharova S, Kaldybekov D, et al. Improving biodegradability of polyvinyl alcohol/starch blend films for packaging applications. *International Journal of Basic and Applied Sciences*. 2014;3(3).
 24. Olewnik-Kruszkowska E, Gierszewska M, Jakubowska E, Tarach I, Sedlarik V, Pummerova M. Antibacterial Films Based on PVA and PVA-Chitosan Modified with Poly(Hexamethylene Guanidine). *Polymers*. 2019;11(12):2093.
 25. *Hydrogels in Medicine and Pharmacy*. CRC Press; 2019.
 26. Mallapragada SK, Peppas NA, Colombo P. Crystal dissolution-controlled release systems. II. Metronidazole release from semicrystalline poly(vinyl alcohol) systems. *J Biomed Mater Res*. 1997;36(1):125-130.
 27. Mansur HS, Sadahira CM, Souza AN, Mansur AAP. FTIR spectroscopy characterization of poly (vinyl alcohol) hydrogel with different hydrolysis degree and chemically crosslinked with glutaraldehyde. *Materials Science and Engineering: C*. 2008;28(4):539-548.
 28. El-Kader MFHA, Elabbasy MT, Adeboye AA, Menazea AA. Nanocomposite of PVA/PVP blend incorporated by copper oxide nanoparticles via nanosecond laser ablation for antibacterial activity enhancement. *Polym Bull*. 2021;79(11):9779-9795.
 29. Rajesh K, Crasta V, Rithin Kumar NB, Shetty G, Rekha PD. Structural, optical, mechanical and dielectric properties of titanium dioxide doped PVA/PVP nanocomposite. *Journal of Polymer Research*. 2019;26(4).
 30. Mydhili V, Manivannan S. Effect of microstructure on the dielectric properties of poly(vinyl alcohol)-poly(3,4-ethylenedioxythiophene) doped with poly(styrenesulfonate) composite films. *J Appl Polym Sci*. 2017;134(34).
 31. Jabbar SA, Khalil SM, Abdulridha AR, Al-Bermany E, Karar A. Dielectric, AC Conductivity and Optical Characterizations of (PVA-PEG) Doped SrO Hybrid Nanocomposites. *Key Eng Mater*. 2022;936:83-92.
 32. Al-Kateb DE, Abdulridha AR. Structural and Optical Properties of (PVA/PVP: Sr_2NO_3) Nanocomposites. *Neuroquantology*. 2021;19(4):27-37.
 33. Feng Q, Dang Z, Li N, Cao X. Preparation and dielectric property of Ag-PVA nano-composite. *Materials Science and Engineering: B*. 2003;99(1-3):325-328.
 34. Aunkor MTH, Raihan T, Prophan SH, Metselaar HSC, Malik SUF, Azad AK. Antibacterial activity of graphene oxide nanosheet against multidrug resistant superbugs isolated from infected patients. *Royal Society open science*. 2020;7(7):200640-200640.